The design and commissioning of a fully elastic model of a uniform container ship

Apostolos Grammatikopoulos*, Joseph Banks, Pandeli Temarel

Maritime Engineering Group, University of Southampton, Boldrewood Innovation Campus, Burgess Rd, SO17 6QF Southampton, United Kingdom

Abstract

Experimental hydroelasticity has not followed the rapid evolution of its computational counterpart. Hydroelastic codes have changed significantly in the past few decades, moving to more detailed modelling of both the structure and the fluid domain. Physical models of ships are, even today, manufactured with a very simplified structural arrangement, usually consisting of a hollow rectangular cross section. Appropriate depiction of the internal structural details ensures that properties relevant to antisymmetric vibration are scaled accurately from the real ship to the model. Attempts to create continuous, ship-like structures had limited success, as manufacturing constraints did not allow for much internal structural detail to be included. In this investigation, the first continuous model of a ship with a detailed internal arrangement resembling a container ship is designed, produced using 3D printing and tested in waves. It is demonstrated that the global responses of the hull in regular head waves agree well with theory and past literature, confirming that such a model can represent the behaviour of a ship. Furthermore, it is found that the model is capable of capturing local responses of the structure, something that would be impossible with "traditional" hydroelastic ship models. Finally, the capability of the model to be used to investigate antisymmetric vibrations is confirmed. The methodology developed here opens a whole new world of possibilities for experiments with models that are tailored to the focus of the investigation at hand. Moreover, it offers a powerful tool for the validation of modern state-of-the-art hydroelastic codes. Ultimately, it creates the next step in the investigation of dynamic responses of ship structures, which contribute significantly to accumulating damage of the hull. Better understanding of these responses will allow designers to avoid over-engineering and use of big safety factors to account for uncertainties in their predictions.

Keywords: additive manufacturing, cellular, container ship, hydroelastic testing, thin-walled girders

1. Introduction

Computational methods to predict the hydroelastic responses of ships have evolved greatly in the past few decades. The initial approaches were 2-dimensional, coupling Timoshenko beam theory with Lewis sections and strip theory [1]. Modern codes tend to be 3-dimensional, using either potential flow solvers [2] or Reynolds-averaged Navier-Stokes solvers [3] for the fluid domain. On the structural side, state-of-the-art involves either a 3D model of shell structure or sophisticated beam modelling [4].

Despite these advancements, the physical models used in hydroelastic experiments have not changed much since the field was established. Models are traditionally manufactured as rigid and subsequently split in segments along the length [5]. The flexibility is then introduced by means of either flexible joints connecting the segments [6] or, more commonly, a flexible backbone [7]. Consequently, the hydrodynamic

*Corresponding author

Email addresses: A.Grammatikopoulos@soton.ac.uk (Apostolos Grammatikopoulos*), J.Banks@soton.ac.uk (Joseph Banks), P.Temarel@soton.ac.uk (Pandeli Temarel)

and structural aspects are completely segregated. More importantly, the structural stiffness is provided either artificially (flexible joints) or from a structure that does not resemble that of a ship in any way (flexible backbone).

The geometry of the structure is not always an issue. In terms of vertical bending, the effects of shear deformation are important but differences can always be taken into account when running the numerical simulations to apply corrections for the full-scale ship. Nevertheless, if the 2-node bending natural frequency of the vessel is appropriately scaled, the relevant mode shape will not change significantly based on the equivalent shear area.

Scaling of a the structure becomes much more challenging when looking at the antisymmetric responses of ships. Torsion causes shear stresses, and the flow of the latter within the cross section is highly dependent on the geometry. Consequently, scaling of aspects such as the torsional constant and the location of the shear centre relies on appropriate depiction of the cross section. It is common practice to use U-shaped backbones [8] or backbones with cut-outs [9] to achieve the correct 2-node vertical bending and 1-node twisting natural frequencies. However, the above does not necessarily ensure correct coupling of horizontal bending and torsion, which can severely affect the mode shapes [10].

To overcome these limitations, a number of investigators have attempted to manufacture continuous models with an internal structure more similar to that of a ship, the so-called *elastic* models. However, manufacturing constraints did not allow for much internal detail to be included and these models consisted of an external shell with transverse bulkheads and deck openings [11, 12, 10, 13]. As a result, the segregation of hydrodynamic and structural aspects was overcome but the shear flow was not appropriately depicted. It was not until quite recently that more advanced manufacturing options became available.

Grammatikopoulos et al., demonstrated that the static and dynamic flexural moduli of 3D printed components can be significantly different, rendering standard 3-point bending tests irrelevant to the design of elastic ship models [14]. An experimental procedure, based on specimen-scale modal testing, was developed that allowed accurate prediction of several natural frequencies of the vessel [15]. Indications regarding the structural damping could also be obtained from the same procedure.

In this investigation, additive manufacturing is used to produce a fully-elastic model of a uniform container ship. The term *fully-elastic* intends to describe a model that is not only continuous and experiencing the loads directly on its hull, but also an internal structure that resembles that of a ship. The design procedure is described, with a brief mention of the vessels that acted as an inspiration. The manufacturing constraints that largely defined the scale of the model and the achievable bending stiffness are discussed, along with the effects of manufacturing uncertainties. The vessel is instrumented, its modal properties are identified and it is finally subjected to towing tank tests in head waves at zero forward speed. The results are compared to 2D hydroelasticity to verify the concept. Effects of the 3-dimensional nature of the structure are presented. Finally, the behaviour in beam and oblique seas is briefly examined to confirm the suitability of the model for such experiments.

2. Model design and production

2.1. Model design

In order to select the vessel to be manufactured as an elastic model, previous investigations that were used as benchmark studies were examined. The most characteristic case was the rectangular barge that was manufactured by Malenica et al. [16] and subsequently used for comparison to a number of simulation techniques (e.g. [17, 18]). One of the major advantages of this vessel was its simple geometry that made its modelling in any kind of simulation environment relatively easy and ensured fair comparison of the hydroelastic response predictions. A second well-known case was the S-175 container ship, several incarnations of which are present in the literature as physical models [11, 12, 19], allowing for comparison not only among computational but also experimental techniques.

The depiction of a real vessel was beyond the scope of the present investigation, which was proof-of-concept. It was decided to combine the best traits of the flexible barge and the S-175 containership into a new model. A rectangular barge with a constant cross-section inspired by a container ship allowed hydroelastic testing of a complex 3D printed section while minimising design complexity.

The volumetric capabilities of the printer largely determined the scale used for the vessel. A minimal number of sections was desired due to the uncertain effects of section joining on the dynamic properties of the model. For the same reasons, it was decided that the cross-section should fit in the build volume of the printer without any transverse division. The resulting maximum breadth of 22 cm was used to define the ratio λ_m between the S-175 model [12] and the barge (for general particulars). All dimensions were then derived by Froude scaling, with the exceptions of the draft and, of course, the stiffness.

Table 1: Principal particulars of the cellular barge. The S-175 container ship data provided for comparison corresponds to model scale [12].

Dimension	S-175	Barge	Units
L (Length)	3.600	1.520	m
B (Beam)	0.523	0.220	m
D (Depth)	0.317	0.130	m
T (Draft)	0.195	0.047	m
Δ (Displacement)	215.40	15.60	kg
C_B (Block Coefficient)	0.5787	1.0000	-
λ (Scale factor)	48.6	115.1	-
f_{2n} (Dry frequency)	8.57	51.8	Hz

A draft directly scaled by λ_m would not produce the appropriately scaled displacement due to the significant increase in block coefficient moving from a slender ship to the barge. The required draft was instead derived by scaling the displacement of the model by λ_m^3. It should be emphasised that λ_m is the scaling factor between the two models and not between the model and the full-scale vessel. Even if the draft was scaled linearly it would not be feasible to achieve the natural frequency of the S-175. The only alternative would be to produce a longer vessel to reduce the natural frequency, but that would mean that the principal particulars of the vessel would not be Froude scaled. Furthermore, the necessary increase in length would significantly increase manufacturing time. Since the natural frequency of the vessel would be too high to become directly excited in the towing tank either way, it was decided that Froude scaling of the main particulars of the vessel and scaling of the displacement was the best option. The resulting vessel's natural frequency would be higher than that of the S175 but its hydrodynamic behaviour in waves and resulting loads would be comparable to the original vessel due to the similarity in principal dimensions. The principal particulars for the vessel are summarised in Table 1.

2.2. Model production

The vessel was produced using ABS with an infill ratio of 99% on an UP box 3D printer, manufactured by *Tiertime*. A uniform thickness of 2.5 mm was used for all longitudinal parts of the structure, which was considered to be very close to the minimum thickness the UP box could print with reasonable accuracy. The size of the deck openings and the dimensional proportions of the structure were based on the S-175 container ship [12] and the cellular arrangement was inspired by real container ships (Figure 1). Each section (total of 11) was built with the longitudinal axis of the vessel coinciding with the z-axis (the layering direction) of the printer. A 4 mm deep frame marked the start of each section, and appropriate slots at the beginning and end of each section ensured that this thickness was shared equally between two subsequent sections (Figure 2). The remaining middle part of the section was prismatic. 10 of the sections were printed with a length of 140 mm whereas the fore section had a length of 120 mm to achieve the required length of 1.52 m.

The sections were joined using an ABS paste made of scrap pieces of the parent material dissolved in acetone. The large size of the prints combined with the high thermal expansion rate of ABS resulted in slight peeling of the corners of the section off the print bed and subsequent curving of the bottom of the print. This did not affect the alignment or the connection between sections but did create small gaps between the sections on the outside corners.This was resolved by application of the aforementioned paste to fill the gaps during the joining process. As the longitudinal parts of the cross section were practically solid and the paste solidifies into ABS after acetone evaporates, this practice intended to produce similar properties and

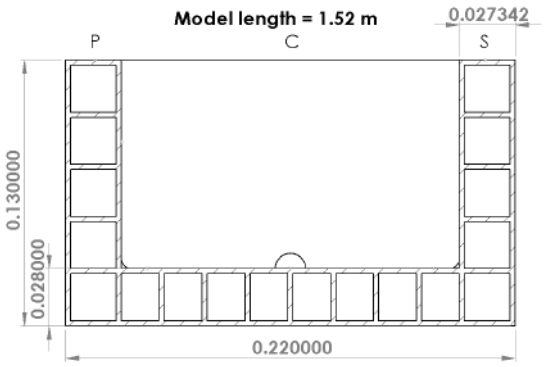

Figure 1: Dimensions of the cross-section of the barge were based on a scaled-down version of the S-175 container ship [12].

ensure longitudinal continuity. A series of bulkheads were added at the same locations as the deep frames, excluding three deep frames where their installation was impossible because of the presence of the tow post. Finally, the vessel surface was sanded and then coated with a clear acrylic paint to improve smoothness and watertight behaviour.

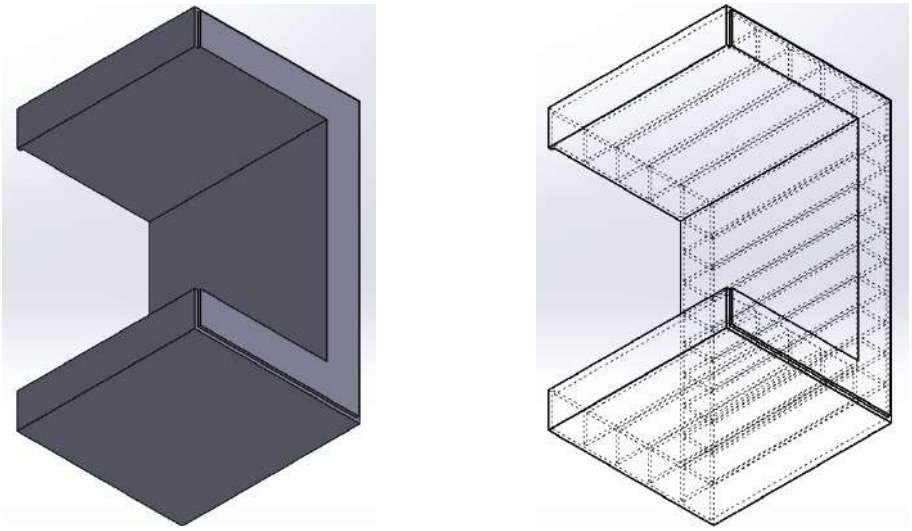

(a) Section (shaded) (b) Section (X-ray)

Figure 2: CAD representation of one of the sections of the model. The deep frame (including a slot to allow easy assembly) is clearly visible in (a), whereas the internal cellular geomery is shown in (b).

As the structure corresponded to a ship, the location along the longitudinal direction was defined by use of *stations*. Within this convention, station 0 corresponded to the stern of the vessel and station 20 corresponded to the bow. Any station in between corresponded to its number times 5% of the length, measured from the stern - for example, station 15 corresponded to $15 \times 5\% = 75\%$ L, measured from the stern. In terms of locations within the cross section, *main deck* refers to the horizontal plating at the top of the structure, on either side; *side wall* refers to the external vertical plating, whereas *inner side* refers to the internal vertical walls. *Port* and *starboard* are the nautical terms for the left and right side of the vessel, respectively. Axes X, Y, and Z correspond to the directions along the length, breadth, and depth of the vessel, respectively.

2.3. Cross-sectional properties

Dimensional measurements were taken throughout the sections of the structure and compared to nominal values. It was observed that uncertainties were much more pronounced for thickness as opposed to larger dimensions. In most cases, thickness average was found to be 10-23% higher than the nominal but with a standard deviation of 1.5-4.3% of the average value. The maximum values for error and standard deviation for the larger dimensions were 1.08% and 0.38%, respectively. The final length of the vessel was found to be 1.525 m, which results in an error of 0.3%.

The geometric inaccuracies described above were a result of an older-generation 3D printer being used for the purposes of the project, which was struggling to produce this level of thickness. Currently available printers would not suffer from these issues and would, in fact, be able to accurately produce structures with a thickness of less than 1 mm.

Table 2: Statistical predictions for the cross-sectional properties of the vessel, based on dimensional measurements and use of a Monte-Carlo simulation.

Property	Mean	SD
Cross-sectional Area (m^2)	3.72E-03	3.70E-05
2^{nd} Moment of Area (m^4)	6.10E-06	6.16E-08
Centroid (vertical) (m)	4.59E-02	3.33E-04

The mean values and standard deviation of various dimensional measurements of the cross section were used as an input to a Monte-Carlo simulation to evaluate the uncertainty over cross-sectional properties. A population of 10000 randomly-generated cross sections was used and results were found to converge after approximately 1000 sections. A summary of the results can be found in Table 2. It was concluded that the variation of cross-sectional properties is not large enough to affect the estimation of vibratory properties of the vessel.

3. Experimental procedure

3.1. Modal testing

The vessel was subjected to modal testing in a free support condition. It was tethered using bungee cords at stations 6 and 14, as due to spacial constraints in the experimental setup it was not possible to tether it exactly at the 2-node vertical bending mode nodes (namely stations 5 and 15). The bungee cords were sufficiently flexible for the rigid natural frequency of the model to be more than an order of magnitude lower than the first flexible natural frequency. The tests were then repeated for the vessel in water, with details of the set up, described below, being the same apart from the boundary conditions.

The roving hammer setup used a PCB-086C03 instrumented hammer (sensitivity: ($\pm$15%) 11.2 mV/N) with a hard plastic tip (white) for the excitation measurement and three PCB-352C22 accelerometers (sensitivity: ($\pm$15%) 1.019 mV/m/s^2, 0.998 mV/m/s^2 and 1.003 mV/m/s^2, respectively) for the response measurement.

The accelerometers were located at station 19 of the ship structure on the starboard side. Two of them were installed on the inner side to measure along the Y-axis. This setup was selected so that further post-processing of the measurements would allow the calculation of translational and rotational acceleration at the midpoint [20]. The vertical locations of these accelerometers (z=0.031 and 0.059 from the bottom, respectively) were selected so that the midpoint coincides with the vertical location of the centroid of the cross-section. The third accelerometer was placed on the main deck to measure along the Z-axis.

All measurements were obtained using a DataPhysics Quattro acquisition system and SignalCalc software and the latter was also used for the calculation of the relevant frequency response functions. For each measurement point, the test was repeated thrice, the frequency response function was calculated for each repetition and an average was produced. The measured frequency range was between 0 and 400 Hz (at a 0.5 Hz step).

Modal testing was split into two phases. In the first one, the ship structure was excited horizontally. The excitation points were located at each station (so every 5% of the ship structure length), starting at station 1 and ending at station 19. For all stations, the excitation point was located at the side wall of the ship structure and exactly below the main deck. Measurements were obtained on both the port and the starboard side.

In the second phase, the vessel was excited vertically. The excitation points were located at the midpoint of the main deck, both for port and starboard side. In this case, not all stations could be excited due to the presence of strain gauges in some of them. Namely, stations 1, 2, 3, 6, 8, 11, 13, 14, 16, 17 and 19 were excited on both sides of the vessel.

The tests above, including both directions of excitation, were repeated with the vessel freely floating in water to identify the wet modal properties.

In order to calculate modal damping, MATLAB function *modalfit* [21] was used. This function takes a frequency response function (or series of frequency response functions) as an input and uses curve-fitting techniques to translate that to a series of natural frequencies and the corresponding damping ratios and mode shapes. Use of this technique ensured that the whole frequency response function, rather than isolated peaks, was taken into account when calculating damping.

3.2. Instrumentation

The model was instrumented with 16 strain gauges and an accelerometer. Measurements in both static and towing tank tests were obtained using a National Instruments cDAQ-9135 Data Logger. Two National Instruments NI-9236 strain gauge modules were used for the strains and a NI-9234 sound and vibration input module for the accelerations. During towing tank tests, measurements for heave and pitch from the tow post sensors were transferred through the locally used amplifying unit to a NI-9205 Voltage module. All the above measurements were obtained using LabVIEW software. The wave probe measurements during the tank tests were obtained through the Lasso software, developed by the Wolfson Unit.

Table 3: Positioning of strain gauges. X refers to stations, Y to port, starboard or centreline and Z to main deck, inner bottom or inner side

#	X	Y	Z
0	5.0	P	MD
1	7.5	P	MD
2	10.0	P	MD
3	12.5	P	MD
4	15.0	P	MD
5	5.0	S	MD
6	10.0	S	MD
7	12.5	S	MD
8	5.0	C	IB
9	7.5	C	IB
10	10.0	C	IB
11	12.5	C	IB
12	15.0	C	IB
13	10.0	P	IS
14	10.0	P	IB
15	10.0	S	IB

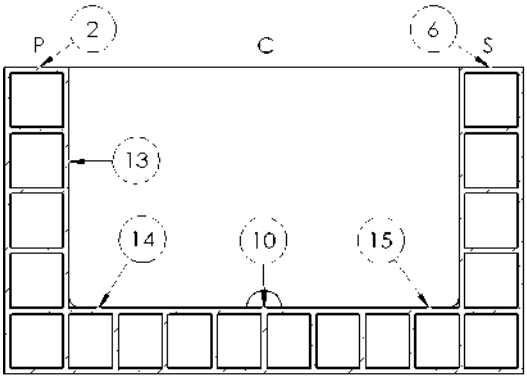

Figure 3: Locations of strain gauges amidships (i.e. station 10.0). Main deck and Inner bottom locations same for other stations (See also Table 3).

The strain gauges used were Micro-Measurements C2A-06-250LW-350 linear quarter-bridge strain gauges with a resistance of 350 Ω and a gauge factor of 2.150±0.5%. Half of the gauges were placed on the main deck, port and starboard. Seven gauges were placed on the inner bottom and the last one was placed on the inner side of the vessel. All strain gauges were placed parallel to the longitudinal axis of the vessel.

Detailed positioning of the gauges is presented in Table 3. The accelerometer used was a PCB-352C33 and was installed on station 0.5, on the centreline.

3.3. Experiments in head waves

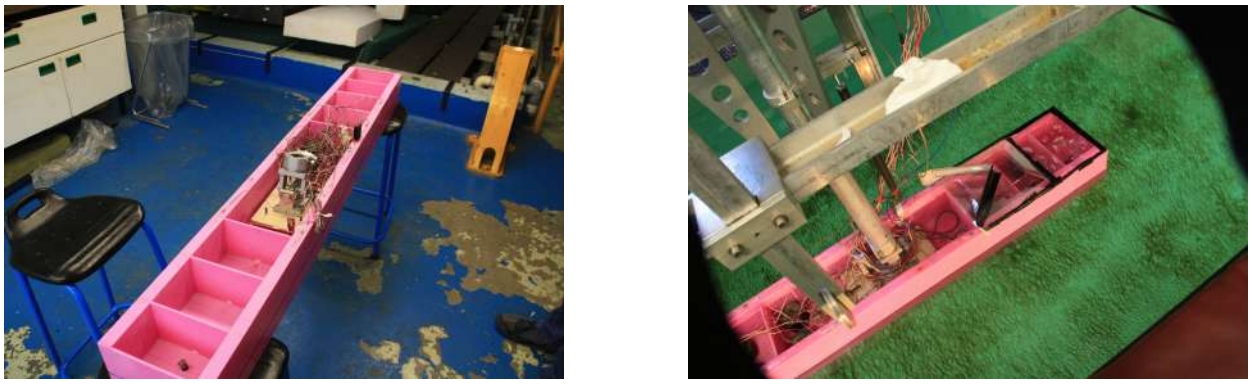

(a) tow post attachment

(b) Forward deck & wave breaker

Figure 4: A tow post, forward deck and wavebreaker were attached to the vessel.

The model was tested in head waves in the Solent University towing tank, for which the particulars are included in Table 4. The tow post was placed at station 12, i.e. 10% fore of the midship section. A plate of plywood 250 mm long and 150 mm wide, connected to the model using captive nuts and threaded bars served as the base for the tow post (Figure 4a).

Table 4: Solent University towing tank size and capabilities

Length	60.0	m
Width	3.7	m
Depth	1.8	m
Maximum velocity	4.0	m/s
Maximum model length	2.0	m

The positions of the ballast masses are presented in Table 5. The above resulted in a displacement of 15.60 kg and zero trim.

Table 5: Positions and masses of ballast masses. All ballast masses were placed on the inner bottom along the centreline.

Station	Mass (kg)
1.0	0.50
2.5	0.50
4.5	0.50
6.5	1.00
8.0	2.00
15.5	1.00
17.5	1.00

Table 6: Wave length ratios and frequencies for the tests in regular waves. A wave height of 0.05 m was used in all cases.

λ/L	ω (rad/s)	f (Hz)
0.6	8.22	1.31
0.8	7.12	1.13
0.9	6.71	1.07
1.0	6.37	1.01
1.1	6.07	0.97
1.2	5.81	0.93
1.3	5.59	0.89
2.0	4.50	0.72

The model was tested without forward speed at a range of wave frequencies and with a constant wave height of 0.05 m which corresponds to H_{wave}/L of 1/30. The wave frequencies were selected based on the λ/L used in [12, 22] for the relevant wave height ratio. The tests were repeated three times for each case.

A deck structure and wave breaker were fitted to avoid water ingress (Figure 4b). The deck structure was made out of thin plastic that was sufficiently flexible to not affect the structural properties of the hull locally. The model mass was measured before and after the testing each day to ensure no invisible water ingress was present. After three days of testing, the mass had increased from 15.6 kg to 15.65 kg using a scale with an accuracy of ±0.025 kg.

The measurements were processed using a windowed Fast Fourier Transform (FFT). The flat top window was used as it was found to produce the most accurate results as far as signal amplitude is concerned, although it creates more spectral leakage than other windows. The response amplitude operators (RAOs) were calculated and results for each run were plotted separately (not averaged for each condition).

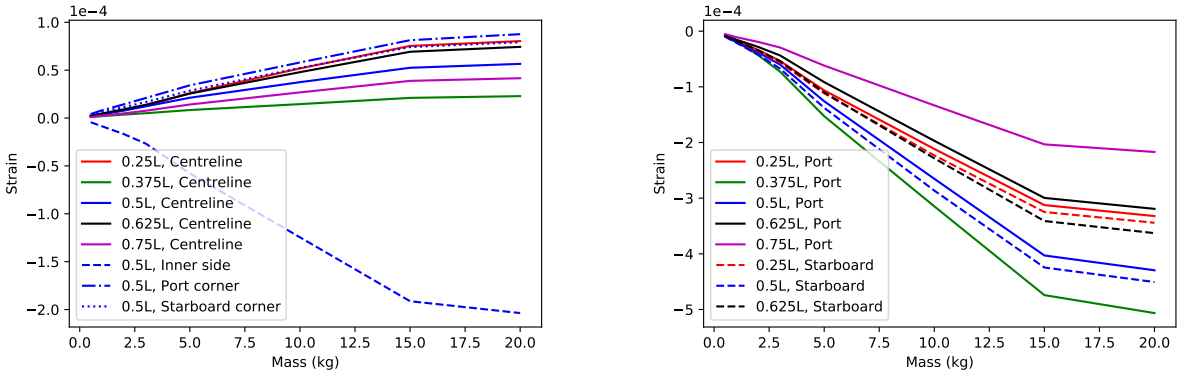

(a) Internal locations

(b) Main deck locations

Figure 5: Strain measurements during static calibration indicated that material behaviour only becomes nonlinear for strains much larger than those experienced during ship bending.

The strains were converted to bending moments using the bending moment/strain coefficients obtained from static tests. These 3-point bending tests were performed by supporting the vessel in a pinned-pinned condition and applying weights on the inner bottom at the tow post location while measuring strains. The results indicated an almost linear material behaviour. A significant change in the slope was observed after the 15 kg point load in all sections and was attributed to material non-linearity, which was expected as stress-strain curves for ABS are of sigmoidal shape (Figure 5). The responses of the vessel in waves, however, should not be affected as they were found to be well below that region in terms of bending moments. The bending moments from the strain measurements and the 2D hydroelasticity predictions were non-dimensionalised using the following equation:

$$C_M = \frac{M}{\rho g L^2 B A_{wave}} \tag{1}$$

As demonstrated previously by the authors [15], the static and dynamic moduli of 3D printed structures can be significantly different. This is likely to affect the accuracy of a bending moment calibration that is performed statically as described above. Within this publication, and in absence of a better alternative, the static calibration results are used, to provide an initial evaluation of the concept through commonly used metrics, such as the non-dimensionalised bending moment. Methods to calibrate the conversion to bending moments through dynamic testing should be developed in the future to ensure sufficient measurement accuracy.

The responses of the vessel were compared to results from a linear 2D hydroelasticity code, based on strip theory and Timoshenko beam theory [1]. The ship was modelled as 20 strips, where the actual mass distribution was used and the flexural modulus was selected to produce, in conjunction with the known second

moment of area, the correct 2-node bending natural frequency. Apart from the dry natural frequencies and mode shapes, the code was used to produce the heave, pitch and bending moment RAOs of the vessel.

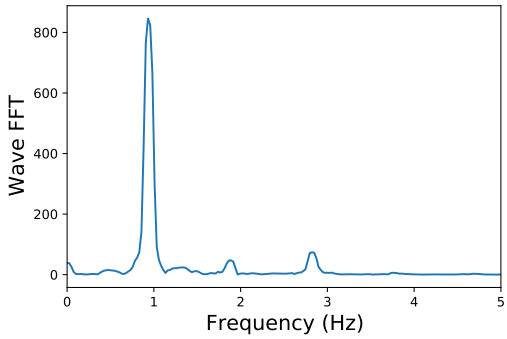

Figure 6: Uncertainties in the experimental process included frequncies other than the nominal contaminating the regular waves produced.

The FFT of a typical regular wave revealed two smaller peaks following the primary peak of the desired frequency (Figure 6). It was observed during the experiments that the waves were interacting with the underside of the raised beaches (positioned down the side of the tank). This may have created additional wave components with a smaller amplitude that radiated out from the side of the tank. Wave elevation was only measured with the model present in the tank, so it is also possible that these higher harmonics are partly caused by the relevant structural responses, generating radiated waves from the stationary model. Nevertheless, the frequency content of the waves should be taken into account if an attempt to replicate the responses in a simulation is performed. Within this study, the wave amplitude used for the calculation of bending moment & motion RAOs was obtained from measurements with the model in the tank, and the potential influence from radiated waves is acknowledged as a source of uncertainty.

The blunt bow of the vessel resulted in significant green water at forward speed and that is why testing was performed at zero forward speed. The same phenomenon was observed when a wave length of 0.6L was tested, as the vessel would crash into the waves rather than ride over them. As the wave probe was located at the same longitudinal location as the bow of the vessel, the wave measurements in these cases were significantly affected. Due to testing with no forward speed, the responses would be, to some extent, also affected by tank wall effect.

4. Results

4.1. Natural frequencies and damping

The measured dry & wet natural frequencies of the vessel and the corresponding wet damping ratios are summarised in Table 7. Statistical values for both were calculated from the different excitation points. As far as the damping ratios are concerned, only results with sufficiently small standard deviation (less than 50%) from the average are presented.

Table 7: Measured natural frequencies and damping ratio for the ballasted model. Damping ratio values correspond to the vessel in water. Higher natural frequencies in vacuo are missing as they could not be accurately identified (see text).

Mode	Dry f_n (Hz)		Wet f_n (Hz)		Damping ratio	
	Mean	SD	Mean	SD	Mean	SD
2VB	51.8	0.7	30.0	0.3	0.0146	0.0025
1HB, 1T	66.8	1.3	46.4	0.3	0.0113	0.0023
2HB, 2T	-	-	54.8	0.7	0.0240	0.0092
3VB	-	-	78.2	0.8	-	-

In a previous investigation, the modal properties corresponding to the vessel without any ballast masses were measured [15]. Ballasting the vessel increased its mass and reduced the natural frequencies, particularly those corresponding to symmetric responses, therefore the values in Table 7 differ noticeably from the ones included in the aforementioned publication. Ballasting also appeared to increase the modal damping significantly, resulting in quite wide peaks in the frequency response function. The latter rendered identification of the higher natural frequencies quite challenging and also led to poor performance of the curve-fitting techniques in general. This can be observed, for example, in the fact that only the first symmetric and first antisymmetric mode in vacuo could be clearly identified.

Some increase in the damping due to ballast masses could be caused by dry friction between the masses and the structure, similar to cargo damping described by Betts et al. [23]. The absence of this phenomenon when testing with backbone models can be explained by the fact that, in those cases, the ballast masses are not in direct contact with the load-bearing, vibrating structure. Still, the damping appeared to have almost doubled when compared to the case of the unballasted model [15], which is an unreasonably large increase. This merits further investigation in the future.

It can be seen in the literature that elastic models produced either using polyurethane foam [24] or ABS plates [12], have particularly increased damping ratio in water, of the order of 0.12 and 0.067, respectively. Segmented models have significantly lower damping ratios, for example 0.009 for flexible joint models [25]. It is claimed, however, that the damping of the real ship is expected to be of the order of 0.015-0.02 [26], agreeing well with the measurements in this investigation.

The frequency response functions of the model in water were found to have more pronounced peaks and higher-order modes could be identified. The wet natural frequencies were further reduced due to the effects of added mass. Uncertainty over the damping ratios increased with mode order, with the standard deviation corresponding to the second antisymmetric mode being almost 40% of the average. Curve-fitting techniques around the 3-node vertical bending natural frequency and beyond performed too poorly to draw any conclusions.

As the presence of fluid around the vessel could not possibly have reduced structural damping, it was concluded that part of the increase compared to the unballasted vessel reported earlier in this section was probably a result of friction between the bungee cords and the model (for tests in vacuo), due to them being tighter around a now heavier model. Measured damping ratios for the dry hull are thus omitted here as interference from the support is almost certain. The magnitude of damping ratios in calm water was comparable to previous measurements from container ship backbone models (e.g [27, 28]).

4.2. RAOs in head waves

Heave and pitch responses showed relatively good agreement with strip theory results, although the code used failed to identify a peak in the heave responses at the area of wave-ship matching (Figure 7a). Discrepancies between measured & predicted rigid body motion responses were attributed to the use of Lewis sections for a vessel with rectangular cross sections and vertical bow and stern walls.

Bending moment measurements were found to agree better with 2D hydroelasticity for the aft half of the vessel (stations 5.0, 7.5 and 10.0). Measurements were found to be less consistent between runs for shorter wave lengths and differences between measurements and predictions also increased for these cases (Figure 8). Green water was observed on the deck of the vessel for these higher frequencies, particularly for λ/L=0.6. The bluff bow of the vessel would crash into these shorter waves and part of the wave would run over the fore deck. Overall, looking at the non-dimensionalised vertical bending moment coefficients, it was observed that the first harmonic component had similar values as the ones measured by Chen [12] for the S-175 container ship.

4.3. Strain distribution throughout the vessel

Both static tests and towing tank tests revealed limited asymmetry between the responses at port and starboard side of the vessel. The difference was, in most cases, of the order of 3% and could be a result of the manufacturing process and material uncertainty. Some asymmetry was also observed in the modal tests but the differences were within the accuracy of the instrumented hammer ($\pm$ 15%)

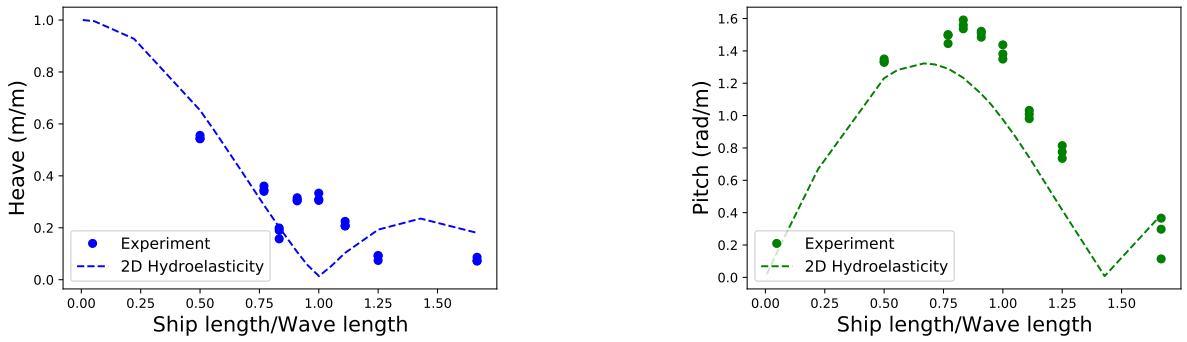

(a) Heave (b) Pitch

Figure 7: Heave and pitch RAOs at no forward speed, comparison between experiments and linear strip theory (where available).

Interestingly, the strain distribution revealed significantly reduced values for inner bottom centreline gauges at stations 10 and 12. Figure 9 includes measurements for a wave length equal to ship length, although similar measurements were observed for other frequencies. This phenomenon was also observed in static tests and was attributed to locally increased stiffness because of the presence of the plywood plate and tow post fitting attached to it (Figure 4a). This would mean that the responses measured in those areas no longer correspond to the global responses of a free-free beam idealisation. This effect was not evident in measurements from the main deck, although comparison with linear strip theory results showed better agreement for the aft stations, possibly resulting from the same added stiffness (Figure 8).

While the stiffness originating from the plywood plate was undesirable, it is probably unavoidable unless a completely free-running model were to be used in an ocean basin. Nevertheless, it demonstrated how the local arrangement of the structure can cause the responses to deviate from beam theory despite originating from global loading. Therefore, this local increase in stiffness illustrates the ability of a complex ship structure to be investigated using 3D printed elastic models.

The strains within the cross section of the model (in this case, amidships) are depicted in Figure 10 as a function of the distance from the cross-section's neutral axis. These measurements are based on the same condition as Figure 9. It was observed that the strain distribution has a linear relationship with the aforementioned distance, with the strain being approximately zero at the neutral axis. This reinforced the argument that the model's behaviour can be approximated well using Timoshenko beam theory.

4.4. Non-linear responses in head waves

Significant excitation of higher order harmonic responses was observed. An example of the relevant isolated signals (obtained by use of a band-pass 1st order Butterworth filter) is depicted in Figure 11. These harmonics were partly the result of higher frequency components in the wave itself (see also Figure 6), which also explains the fact that the 3rd harmonic response had a higher amplitude than the 2nd harmonic response (same pattern observed in the waves). It can be easily observed, however, that harmonic components of much higher order (e.g. 5th), were of similar magnitude to the second harmonic component. The same applied for much higher-order components, with the 15th harmonic being of similar magnitude to the 6th. Components of the response beyond 6th order were omitted from the figure to avoid making it illegible by overcrowding it.

The 2-node vertical bending and 3-node vertical bending components were also present in the FFT of the response. It was demonstrated, however, that, even in still water and with a stationary carriage (a testing condition used as a zero/baseline), the 3-node bending mode was excited to a similar extent and the 2-node bending mode was also excited significantly. These responses were, consequently, partly excited by some type of interference, although its source was not identified with certainty. It was confirmed, however, that while testing the model in a different facility (the tests had a different purpose but included both static

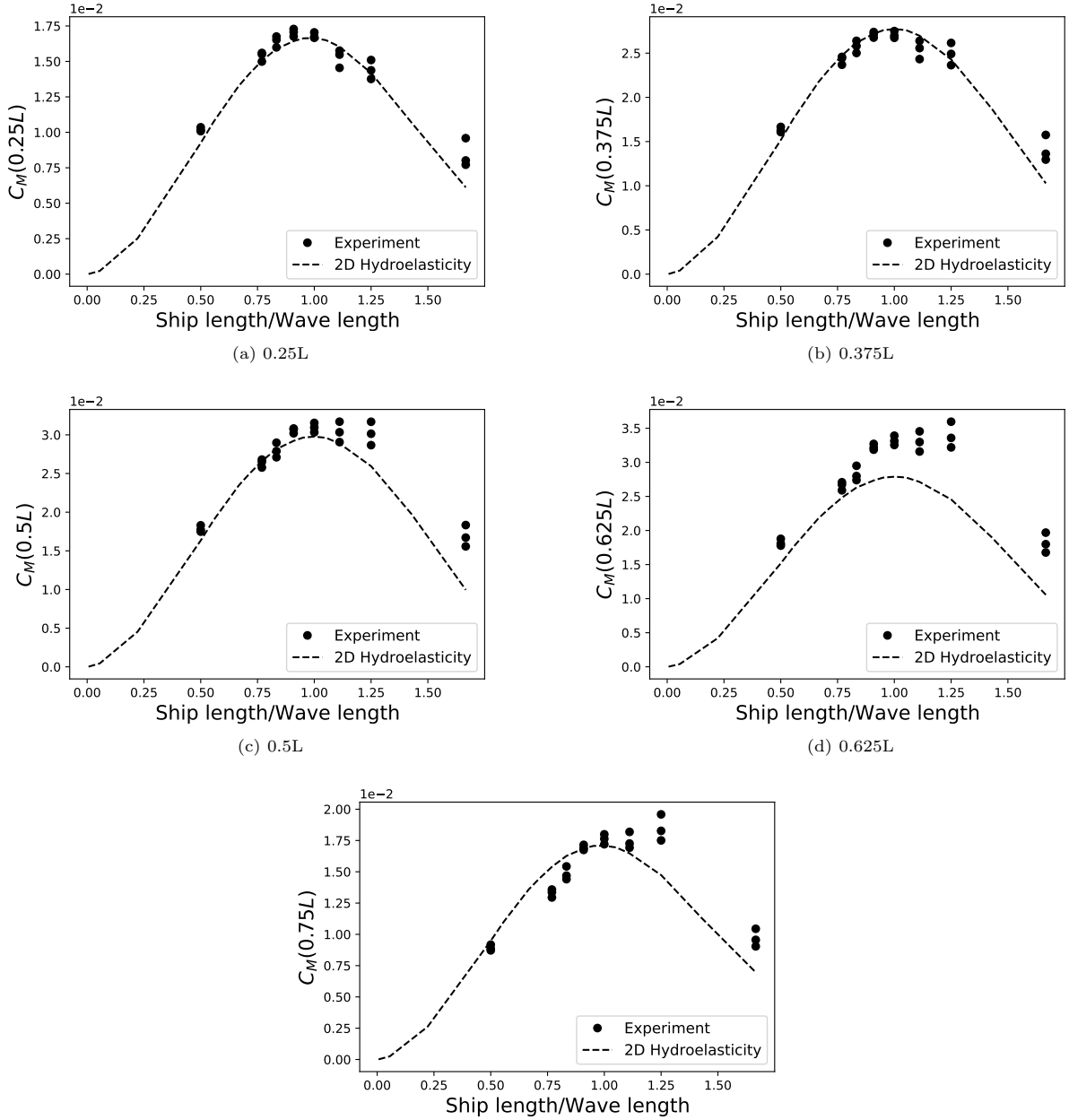

(a) 0.25L

(b) 0.375L

(c) 0.5L

(d) 0.625L

(e) 0.75L

Figure 8: Bending moment RAOs at zero forward speed agree well with linear strip theory, especially towards the aft part of the vessel.

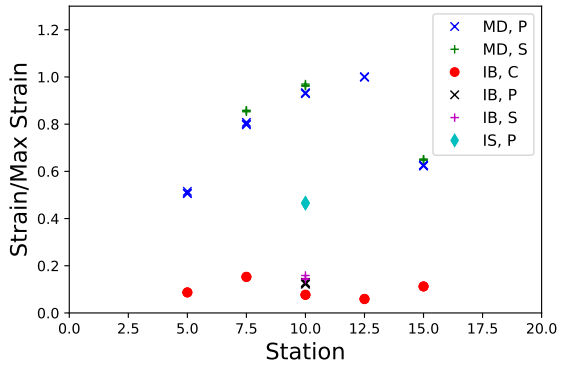

Figure 9: Strain distribution reveals limited asymmetry in the responses as well as locally increased stiffness at the inner bottom, around the tow post attachment. Explanation of the abbreviations in the legend is included in Table 3.

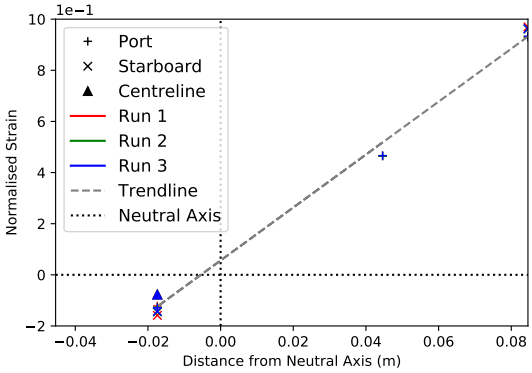

Figure 10: Strain distribution amidships indicated linear distribution of stress as a function of distance from the neutral axis, agreeing with beam theory. Strain was normalised by dividing by the maximum strain measured in each run.

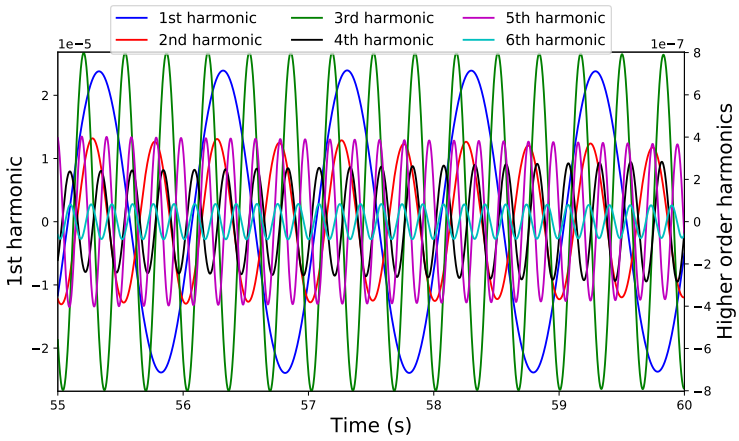

Figure 11: Isolated strain signal of the components of the response, including 1st order and higher order harmonics. The nominal wave frequency, in this case, was 1.01 Hz, corresponding to wave-ship matching.

measurements and a few wave cases at zero forward speed) these components of the response disappeared. In the cases of slamming, approximately half of the magnitude of the 2-node bending response seemed to result from slamming but it was impossible to isolate one component from the other. Consequently, no definite conclusions regarding the magnitude of whipping responses could be drawn.

The non-dimensionalised 2nd and 3rd order harmonic components were found to be of similar magnitude to what has been observed in the literature (e.g. by [12]). The measured amplitudes for different wave frequencies are summarised in Figure 12. The results seem less organised than what has been previously reported in most investigations and feature similarities and differences regarding the patterns. Firstly, the responses were found to have a local maximum around the wave-ship matching area. This was more pronounced for the 3rd harmonic and particularly at the fore part of the vessel. The most significant inconsistencies with previous experience were the large magnitude of the 2nd harmonic component for a wave frequency corresponding to L/λ=0.5 and, similarly, for the 3rd harmonic component and a wave frequency corresponding to L/λ=0.77. Although there is currently no certain explanation for these quite pronounced peaks, it should be emphasised that uncertainties were increased not only because of the 2nd and 3rd harmonic components being present in the wave (as mentioned earlier) but also because the vessel was stationary, resulting in radiated waves reflecting off the tank walls and interacting with the model.

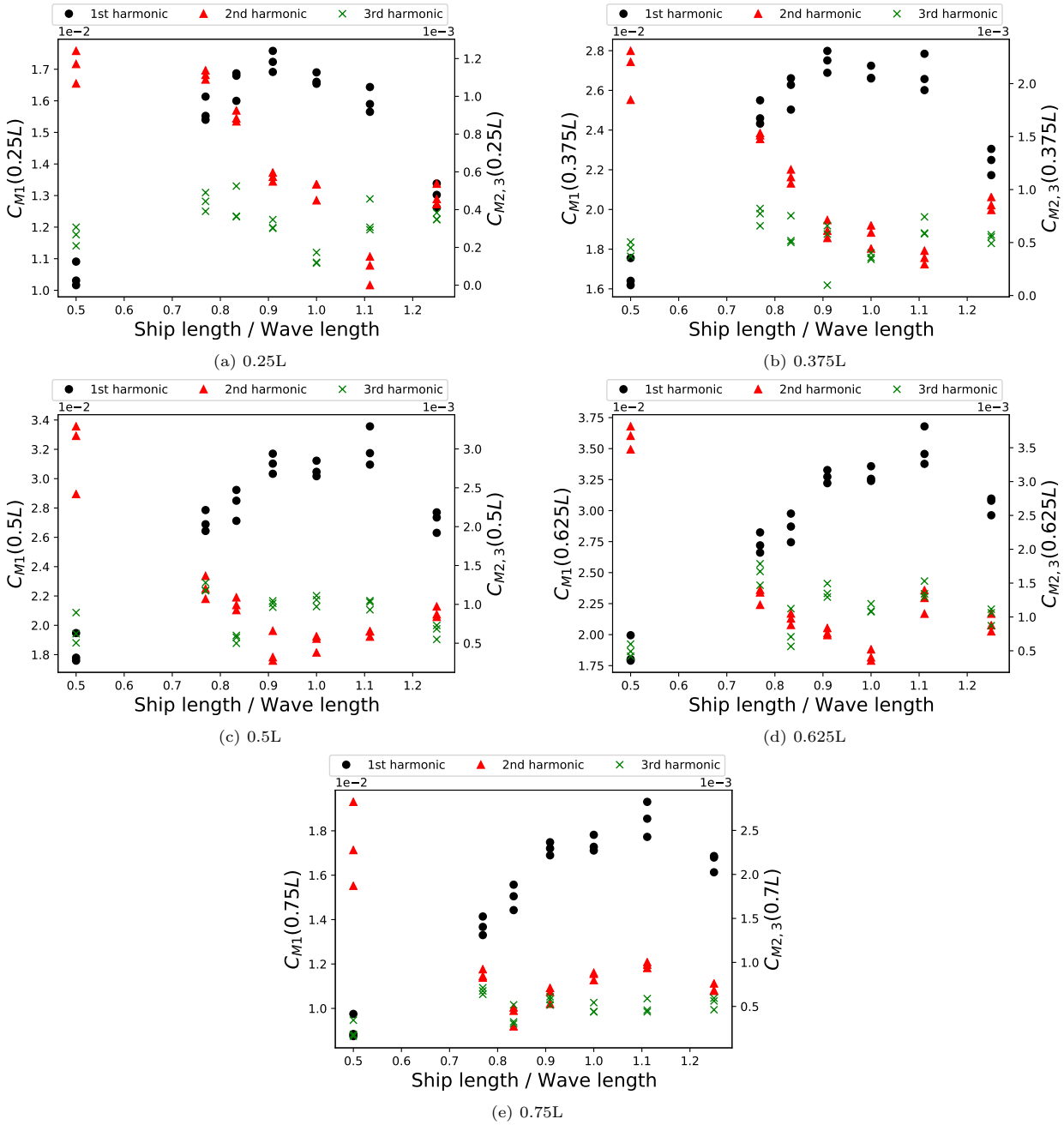

(a) 0.25L

(b) 0.375L

(c) 0.5L

(d) 0.625L

(e) 0.75L

Figure 12: Non-dimensional bending moments at zero forward speed, corresponding to the 1st, 2nd and 3rd harmonic components.

5. Experiments in beam and oblique waves

Although wet antisymmetric responses were not the focus of this investigation, a small number of experiments in beam and oblique seas were performed to determine whether these responses would be measurable on a 3D printed elastic model. As discussed in the introduction, antisymmetric responses are one of the most likely areas to apply this concept. A continuous model with an internal structure resembling a ship can depict the correct distribution of torsional stiffness as well as location of shear centre. These two combined ensure not only appropriate coupling of horizontal bending and torsion but also accurately scaled mode shapes (and as has been previously demonstrated, accurately scaled natural frequencies as well [15]).

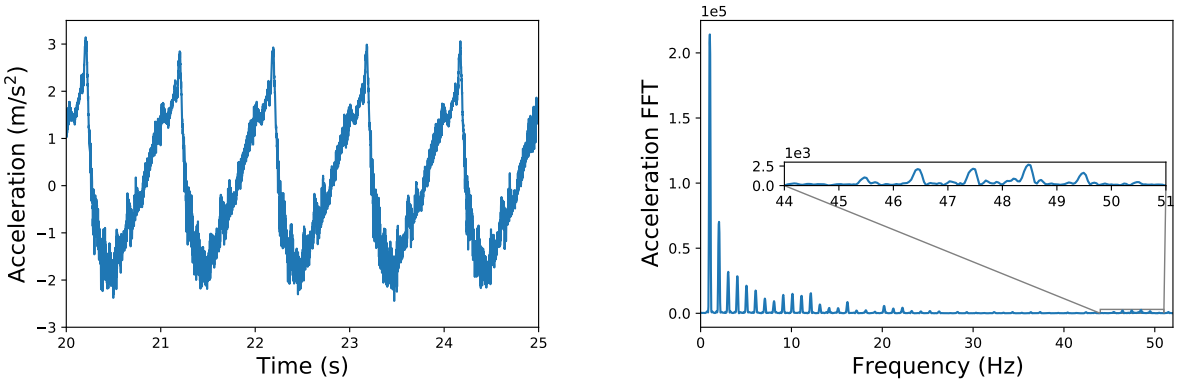

(a) Time signal

(b) FFT

Figure 13: Extract of the acceleration time signal and the corresponding FFT, for tests of the model at a wave angle of 112deg.

A number of limitations in the set-up of the experiments affected the measurements obtained. Firstly, due to the model being tested in a towing tank rather than an ocean basin, the experiments could only be performed at zero forward speed. Secondly, restrictions in the angle of the tow post did not allow for the usual 30˚and 60˚oblique wave angle cases to be tested. Wave angles of 112˚and 156˚were tested instead (in addition to beam seas). The fact that the oblique waves were not approaching the vessel from the the stern was not a problem, in this case, as the geometry of the model's bow and stern were identical and there was no forward speed.

The last limitation was due to the fact that no shear strain gauges were installed on the model. Antisymmetric responses tend to be twist-dominated and direct strains (caused by horizontal bending and warping) are difficult to measure. In the absence of such sensors, an accelerometer was installed near the stern of the model (station 1), measuring in the transverse direction, so as to capture twisting and horizontal bending but not vertical bending. The accelerometer was installed on the inner side of the hull, just below main deck level. Due to time constraints only one wave frequency was tested and this was arbitrarily selected to correspond to ship-wave matching and a wave height of 0.05 m.

The 1-node torsion mode was excited in all cases. Figure 13 depicts the time signal and the FFT for one of the test repetitions of the 112˚case. The frequency content of the response contains significant high frequency components, mostly resulting from higher-order harmonics of the wave frequency. Nevertheless, the excitation of the first antisymmetric mode is clearly visible in the FFT of the signal, even if the magnitude of the relevant peaks is much smaller than, for example, that corresponding to the first harmonic, demonstrating the ability of the 3D printed elastic model to be used to investigate antisymmetric responses. It should be emphasised, at this point, that part of the lower-frequency components of the signal originates from roll motions that can increase the relevant magnitude remarkably.

6. Conclusions

Within this investigation, the first fully-elastic model of a ship was designed, produced and tested. The vessel was manufactured using 3D printing and featured a cellular cross section inspired by modern container ships. Challenges regarding the design and production and ways to overcome them were discussed. Comparison against 2D hydroelasticity found the global responses of the model agreeing with existing theory and the concept was thus verified. Furthermore, flexible symmetric responses also agreed with existing literature, including the first three harmonics of the bending moment. It was further demonstrated that the vessel is capable of capturing local responses of the structure, which would be impossible with segmented models. Finally, brief testing in beam and oblique seas illustrated the capability of such a model to be used to measure antisymmetric responses.

Acknowledgements

The present investigation was funded by the Lloyd's Register Foundation University Technology Center on Ship Design for Enhanced Environmental Performance. Financial support was also received from the EPSRC Doctoral Training Partnership (DTP 15, Grant reference: EP/M508147/1).

References

[1] R. E. D. Bishop and W. G. Price, *Hydroelasticity of ships*. Cambridge University Press, 1979.
[2] S. E. Hirdaris, G. W. Price, and P. Temarel, "Two- and three-dimensional hydroelastic modelling of a bulker in regular waves," *Marine Structures*, vol. 16, no. 8, pp. 627–658, 2003.
[3] P. Lakshmynarayanana and P. Temarel, "Application of CFD and FEA coupling to predict dynamic behaviour of a flexible barge in regular head waves," *Marine Structures*, vol. 65, pp. 308–325, may 2019.
[4] I. Senjanović, S. Tomašević, and N. Vladimir, "An advanced theory of thin-walled girders with application to ship vibrations," *Marine Structures*, vol. 22, no. 3, pp. 387–437, 2009.
[5] A. Marón and G. K. Kapsenberg, "Design of a ship model for hydro-elastic experiments in waves," *International Journal of Naval Architecture and Ocean Engineering*, vol. 6, pp. 1130–1147, jan 2014.
[6] J. Lavroff, M. R. Davis, D. S. Holloway, and G. A. Thomas, "Wave slamming loads on wave-piercer catamarans operating at high-speed determined by hydro-elastic segmented model experiments," *Marine Structures*, vol. 33, pp. 120–142, 2013.
[7] Y. Kim and J. H. Kim, "Benchmark study on motions and loads of a 6750-TEU containership," *Ocean Engineering*, vol. 119, pp. 262–273, 2016.
[8] B. W. Kim, K.-H. Kim, Y. S. Kim, and S. Y. Hong, "Torsion Moment Conversion Methods in Model Test With U-shape Backbone," vol. 3, pp. 782–791, 2014.
[9] S. Zhu, M. Wu, and T. Moan, "Experimental investigation of hull girder vibrations of a flexible backbone model in bending and torsion," *Applied Ocean Research*, vol. 33, no. 4, pp. 252–274, 2011.
[10] H. Houtani, Y. Komoriyama, S. Matsui, M. Oka, H. Sawada, Y. Tanaka, and K. Tanizawa, "Designing a hydro-structural model ship to experimentally measure its vertical-bending and torshional vibrations," *Journal of Advanced Research in Ocean Engineering*, vol. 4, no. 4, pp. 174–184, 2018.
[11] I. Watanabe, M. Ueno, and H. Sawada, "Effects of Bow Flare Shape to the Wave Loads of a container ship," *Journal of the Society of Naval Architects of Japan*, vol. 1989, no. 166, pp. 259–266, 1989.
[12] R.-Z. Chen, S.-X. Du, Y.-S. Wu, J.-R. Lin, J.-J. Hu, and Y.-L. Yue, "Experiment on extreme wave loads of a flexible ship model," in *Practical Design of Ships and Other Floating Structures. Proceedings of the Eighth International Symposium on Practical Design of Ships and Other Floating Structures*, vol. 2, pp. 871–878, 2001.
[13] T. Fukasawa, Y. Yamamoto, M. Fujino, and S. Motora, "Motion and Longitudinal Strength of a Ship in Head Sea and the Effects of Non-Linearities (4th Report)," *Jour. of the Society of Naval Architects of Japan, No.143*, vol. 150, pp. 308–314, 1981.
[14] A. Grammatikopoulos, J. Banks, and P. Temarel, "Experimental dynamic properties of ABS cellular beams produced using additive manufacturing," in *ECCM18 - 18th European Conference on Composite Materials*, (Athens, Greece), 2018.
[15] A. Grammatikopoulos, J. Banks, and P. Temarel, "Prediction of the vibratory properties of ship models with realistic structural configurations produced using additive manufacturing," *Marine Structures*, vol. 73, 2020.
[16] Š. Malenica, B. Molin, F. Remy, and I. Senjanović, "Hydroelastic response of a barge to impulsive and non-impulsive wave loads," in *Proceedings of the 3rd International Conference on Hydroelasticity in Marine Technology*, sep 2003.
[17] F. Remy, B. Molin, and A. Ledoux, "Experimental and numerical study of the wave response of a flexible barge," 2006.
[18] Y. Kim, K.-H. Kim, and Y. Kim, "Time domain springing analysis on a floating barge under oblique wave," *Journal of Marine Science and Technology*, vol. 14, no. 4, pp. 451–468, 2009.
[19] N. Fonseca and C. Guedes Soares, "Experimental investigation of the nonlinear effects on the vertical motions and loads of a containership in regular waves," *Journal of Ship Research*, vol. 48, no. 2, pp. 118–147, 2004.
[20] D. J. Ewins, "Modal Testing: Theory, Practice and Application," p. 562, 2000.

[21] A. Arda Ozdemir and S. Gumussoy, "Transfer Function Estimation in System Identification Toolbox via Vector Fitting," *IFAC-PapersOnLine*, vol. 50, pp. 6232–6237, jul 2017.
[22] Y.-S. Wu, R.-Z. Chen, and J.-R. Lin, "Experimental technique of hydroelastic ship model," in *Proceedings of the Third International Conference on Hydroelasticity, Oxford, UK, September*, pp. 15–17, 2003.
[23] C. Betts, R. E. D. Bishop, and W. G. Price, "A Survey of Internal Hull Damping," *RINA Supplementary Papers*, no. 119, pp. 125–142, 1976.
[24] I. Watanabe and H. Sawada, "Effects of the elastic responses to the longitudinal bending moment in two-directional waves," *Japanese Society of Naval Architects*, vol. 158, 1985.
[25] G. Storhaug, "The measured contribution of whipping and springing on the fatigue and extreme loading of container vessels," *International Journal of Naval Architecture and Ocean Engineering*, vol. 6, pp. 1096–1110, 2014.
[26] G. Storhaug, Q. Derbanne, B.-K. Choi, T. Moan, and O. A. Hermundstad, "Effect of Whipping on Fatigue and Extreme Loading of a 13000Teu Container Vessel in Bow Quartering Seas Based on Model Tests," in *Proceedings of the 30th International Conference on Ocean, Offshore and Arctic Engineering*, (Rotterdam, The Netherlands), pp. 1–10, 2011.
[27] M. Wu, E. Lehn, and T. Moan, "Design of a segmented model for ship seakeeping tests with hydroelastic effects," in *Proceedings of the 6th International Conference on Hydroelasticity in Marine Technology*, (Tokyo, Japan), pp. 135–144, 2012.
[28] S. Zhu and T. Moan, "Nonlinear effects from wave-induced maximum vertical bending moment on a flexible ultra-large containership model in severe head and oblique seas," *Marine Structures*, vol. 35, pp. 1–25, jan 2014.